Fundamentals of Polymer Coagulation

YVES TERMONIA*

Central Research and Development, Experimental Station, E.I. du Pont de Nemours, Inc., Wilmington, Delaware 19880-0356

SYNOPSIS

Polymer coagulation is studied by a Monte Carlo diffusion model in which coagulant, solvent, and polymer particles move on nearest neighbor lattice sites according to the change in local interaction energy. Our approach has allowed, for the first time, to describe the coagulation process beyond the initial quench state and to reproduce the wide variety of different polymer structures that can be obtained, ranging from dust- to finger- to sponge-like morphologies. We show that these morphologies are fully controlled by the coagulation rate which is itself strongly dependent on the degree of miscibility between solvent and coagulant. © 1995 John Wiley & Sons, Inc.

Keywords: model • polymer • evaluation

INTRODUCTION

Polymer coagulation defines the process by which a polymer solution is quenched in an aqueous nonsolvent, leading to solvent–nonsolvent exchange and polymer precipitation. That process constitutes the most important step in the formation of polymeric materials through the solution processing route. It is therefore at the basis of a wide range of polymer processes including wet spinning,[1] fibridation,[2,3] and membrane formation.[4]

Solution processing/coagulation considerably simplifies manufacturing technology and often results in low-cost polymer production. A major drawback of solution processing, however, is that the coagulation step often results in the formation of large tear-dropped macrovoids (fingers) in the wet polymer gel. These voids are extremely difficult to eliminate and they usually remain within the polymer structure regardless of all subsequent consolidating steps. Their presence in the final product severely limits mechanical properties and adversely affects membrane performance.

In spite of its importance, the kinetics of polymer coagulation and finger formation is not well understood. Earlier studies have suggested that fingering instabilities are caused by gradients in interfacial tension resulting from solvent/nonsolvent exchange at the interface.[5,6] The possibility of these so-called "Marangoni" instabilities[7] was later discounted by Ray et al.[8] who contended that their growth rate is much too low. Using linear stability analyses, these authors instead suggested that fingers originate in spatial structures caused by the steep concentration gradients at the polymer interface. In another proposed mechanism,[9] details of the concentration profiles were neglected and fingers were attributed to local increases in solvent flow due to uneven film shrinkage. Other explanations[10] were based on mechanical rupture of the skin which allows the coagulating agent to burst into fast growing fingers extending deep inside the polymer solution. The latter mechanism, however, failed to explain the strikingly regular shape and spacing of the fingers.

Finger formation obviously occurs under far from equilibrium conditions, which therefore casts doubt on the validity of the linear stability analyses of refs. 8–9. For that reason, a large body of research has focused instead to the very early stages of coagulation, *before the onset of phase separation.* These studies were aimed at deriving analytical diffusion equations for the mass transfer paths in the thermodynamic equilibrium phase diagram. That body of research is based on the premise that a detailed knowledge of the location of those paths with respect to the liquid miscibility gap plays a controlling role

* To whom correspondence should be addressed.

Journal of Polymer Science: Part B: Polymer Physics, Vol. 33, 279–288 (1995)
 CCC 0887-6266/95/020279-10

in the determination of the ultimate polymer structure. Earlier studies of mass transfer paths[11] were limited to binary solvent-polymer systems and assumed the solvent leaves by evaporation. The first comprehensive solvent-polymer-coagulant model was proposed by Cohen et al.[12-14] The model clearly revealed the large increases in polymer concentration ahead of the coagulation front. The approach was later refined by Reuvens et al.[15-17] and by Yilmaz, McHugh, and Tsay.[18-20]

The derivation of analytical equations for diffusion in phase separating systems is a formidable task of great complexity. For that reason, all the models described above[11-20] had to resort to several simplifying assumptions: (1) the diffusion process is purely one-dimensional; (2) thermodynamic equilibrium is always preserved at the bath-polymer interface; (3) phase separation is not considered and is assumed to occur through nucleation and growth (i.e., the rate of solvent/nonsolvent exchange is infinitely slow). It is quite unlikely, however, that sudden immersion of a polymer solution in a coagulant results in a mass transfer process that can be fully described by a sequence of equilibrium compositions on a ternary phase diagram. Rather, polymer coagulation is a *nonequilibrium* process which is controlled by the *rate* of solvent–coagulant exchange through the interface. This is particularly true since a dense polymer skin usually forms at the onset of immersion in the coagulant. Finally, we note that all the models of refs. 11–20 have made attempts at predicting conditions under which the final polymer structure is "dense" or "porous." These predictions were based on the tacit assumption that detection of phase separation in the ternary phase diagram invariably suggests pore formation in the ultimate structure. However, as was cautioned in ref. 12, phase separation is a necessary but not sufficient condition for pore formation and a two-phase structure may easily coalesce to a denser film at later stages of the coagulation process.

In view of the great difficulties associated with analytical attempts to describe the development of polymer structure during coagulation, we resort, in the present work, to a computer simulation of the ternary diffusion process. Our approach is based on previous work[21-25] for the description of transport in strongly interacting molecular systems. In our treatment, the coagulation process is simulated on a lattice[21,22] whose sites represent either a nonsolvent, a solvent or a polymer particle. We assume equal molar volumes for the three components.[23] Diffusion on the lattice is described through a Monte Carlo process of particle exchanges on nearest neighbor sites, the probability for a single event being weighted by the Boltzmann exponent of the change in local energy.[23-25] These energy changes are themselves obtained from a set of pair interaction parameters that are easily extracted from binary mixture data.[24,25] Our model has allowed, for the first time, to describe the coagulation process beyond the initial quench state and to reproduce the wide variety of different polymer structures that can be obtained, ranging from dust- to finger- to sponge-like morphologies. A brief account of our approach has been given in ref. 26.

MODEL

For simplicity, our approach is limited to a two-dimensional geometry similar to that encountered in typical experimental studies. In these studies, a drop of polymer solution is placed between two microscope slides and the coagulant is introduced near the edge.[10,27,28] Our two-dimensional model of polymer coagulation is schematically depicted in Figure 1a. The polymer solution is represented by a lattice of sites which are filled-in, according to the polymer weight fraction, by either a solvent or a polymer particle. The bottom five rows of the lattice are filled-in with coagulant particles. Coagulant, solvent and polymer particles are referred to by indexes 1, 2, and 3, respectively. The diffusion of the coagulant into the polymer solution is simulated as follows. We start by picking, at random, a pair of particles—i and j—on nearest neighbor lattice sites. Denoting by α the local environment for that pair, the rate for an exchange $ij \rightarrow ji$ within α is calculated from[21,23]

$$\upsilon_{ij\rightarrow ji,\alpha} = \tau_{i,j}^{-1} \exp[\beta(E_{ij,\alpha} - E_{ji,\alpha})/2] \qquad (1)$$

in which $\tau_{i,j}^{-1}$ is related to the mutual diffusion coefficient, $D_{i,j}^{\infty}$, of i and j particles *at infinite dilution* through[23]

$$D_{i,j}^{\infty} = \tau_{i,j}^{-1} (\delta x)^2 \qquad (2)$$

where δx denotes the unit lattice length. In eq. (1), all the effects of particle interactions are relegated to the Boltzmann exponent of (half) the energy difference between initial and final states for the pair. That functional form for the dependence of rate on local energy change is guided by the requirement of commutativity of the individual two-particles exchanges.[23] Using eq. (1), a probability for exchange is then obtained through

$$P_{ij\rightarrow ji,\alpha} = \upsilon_{ij\rightarrow ji,\alpha} / \upsilon_{\max} \qquad (3)$$

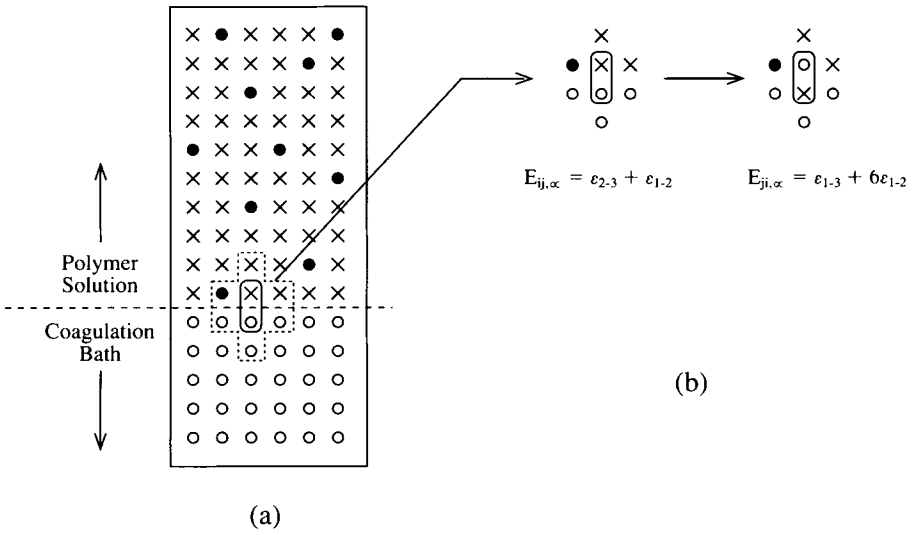

Figure 1. Schematic representation of our lattice model for diffusion of a coagulant into a polymer solution. The polymer, the solvent and the coagulant particles are denoted by symbols ●, ×, and ○, respectively. The diffusion process is simulated through a series of two-particles exchanges on nearest neighbor lattice sites. The rates of exchange are obtained from eq. (1) in which $E_{ij,\alpha}$ and $E_{ji,\alpha}$ are the interaction energies of the pair with nearest neighbor particles, before and after the exchange (see Fig. 1a). As diffusion proceeds, the coagulant/polymer interface (dashed line) moves upward and, since the coagulation bath is assumed to be infinite, the lattice sites below that interface are being continuously replenished with coagulant particles (see text).

in which υ_{max} denotes the highest rate of exchange among all the pairs on the lattice. Having determined the probability p for an exchange $ij \rightarrow ji$ [eqs. (1)–(3)], a random number is generated and the move is allowed if that number falls below p. After each visit of a pair and whether the pair is allowed to exchange or not, the overall "time" t is incremented by $1/[\upsilon_{max} \cdot n]$ in which n denotes the total number of pairs on the lattice.[29] As the coagulant diffuses into the polymer solution, individual polymer particles phase separate into small clusters which also are mobile and aggregate into larger clusters. In our process, small clusters move through a series of one-lattice-step displacements of entire rows or columns of polymer particles (see Fig. 2). The rate of displacement of a row or a column is assumed to be the same as that for a single particle, eq. (1), except for the presence of a prefactor which is chosen inversely proportional to the total number of particles involved in the displacement.[30] Admittedly, other choices of that prefactor are possible. Our model results however reveal that details of the cluster diffusion process are of lesser importance than the choice of values for the pair interaction energies ε. We note also that our full treatment of these interaction energies makes the diffusion coefficients $D_{i,j}$ *at finite dilution* strongly concentration dependent,[23-25] in agreement with experiment and previous continuum diffusion models.[14-20]

A last remark is in order. In order to mimic as well as possible the experimental situation, we assume that the coagulating bath is infinitely large compared to the solvent/polymer system. Thus, solvent particles diffusing into the bath to a depth of more than 5 lattice units with respect to the poly-

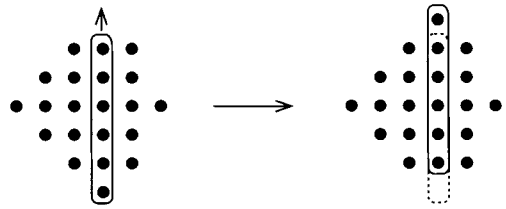

Figure 2. Model representation of the diffusion of polymer clusters. In our process, clusters move through a series of one-lattice-step displacements of entire rows or columns of polymer particles. The rate of displacement of a row or column is the same as that for a single particle [eq. (1)], except for the presence of a prefactor which is made inversely proportional to the total number of particles involved in the displacement.

mer/bath interface are systematically removed from the lattice and replaced by coagulant particles. A full treatment of the case in which the exiting solvent remains in contact with the interface will be the subject of future work.

MODEL PARAMETERS AND TERNARY EQUILIBRIUM PHASE DIAGRAM

Application of the model described above requires a detailed knowledge of the three pair interaction energies $\varepsilon_{1\text{-}2}$, $\varepsilon_{1\text{-}3}$, and $\varepsilon_{2\text{-}3}$ between the coagulant, solvent, and polymer particles. As stated in the Introduction, values of these parameters can be easily determined from binary mixture data.[24,25] The purpose of the present work, however, is not to limit ourselves to a particular coagulant/solvent/polymer system but, rather to present a systematic investigation of the effect of each of these parameters on the final polymer structure. In order for such a study to be meaningful, however, prior knowledge of the range of values of these parameters is essential. In the present section, we turn to an estimation of the interaction energies ε for the coagulation of Nomex®, an aromatic polyamide commercialized by DuPont. The polymer dissolves in *N*-methylpyrrolidone (NMP) and is commonly precipitated in water. The $\varepsilon_{1\text{-}2}$, $\varepsilon_{1\text{-}3}$, and $\varepsilon_{2\text{-}3}$ values for the system water(1)/NMP(2)/Nomex®(3) will be evaluated here for a coordination number $\kappa = 8$, using the method of refs. 23–25. Graduate cooling of a 50/50 solution of NMP in water shows an onset of phase separation at 7°C.[31] Fitting those data to the critical solution temperature predicted in refs. 23–25 for a binary mixture leads to $\varepsilon_{1\text{-}2} = 0.274$ kT units at room temperature. In the absence of any binary mixture data for the pairs water(1)/Nomex®(3) and NMP(2)/Nomex (3), we set $\varepsilon_{2\text{-}3} = 0$ and elect to determine $\varepsilon_{1\text{-}3}$ from the ternary equilibrium phase diagram. An algorithm for estimating the spinodal curve for a given set $\varepsilon_{1\text{-}2}$, $\varepsilon_{1\text{-}3}$, and $\varepsilon_{2\text{-}3}$ values has been presented in ref. 24. A curve-fitting of the calculated spinodal to the actual binodal taken from ref. 28 leads to $\varepsilon_{1\text{-}3} = 1$ kT unit.[32] The calculated spinodal curve is presented in Figure 3. Note that the curve intersects the Nomex/water axis at two points that are equidistant of the 50/50 composition because of our assumption[23] of equal volumes for water and Nomex particles.

All the pair interaction energies ε determined above are for a coordination number $\kappa = 8$. Since the present model study is for a square lattice with $\kappa = 4$, the ε values need to be suitably normalized.

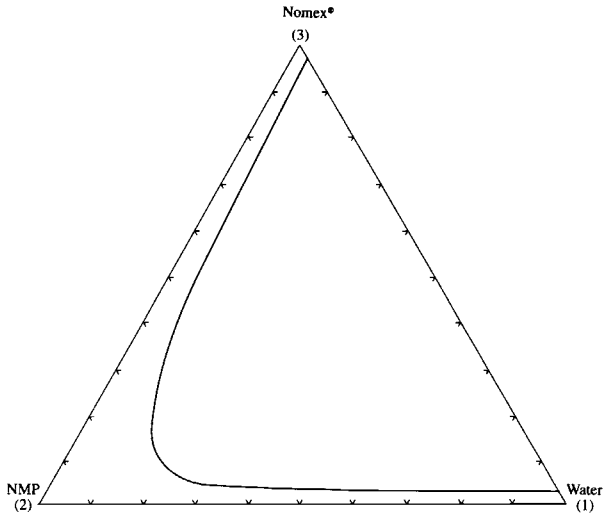

Figure 3. Calculated spinodal curve for the system water(1)/NMP(2)/Nomex®(3). The curve was obtained using an algorithm described in Ref. 24. The figure is for a coordination number $\kappa = 8$, together with $\varepsilon_{1\text{-}2} = 0.274$, $\varepsilon_{2\text{-}3} = 0$, and $\varepsilon_{1\text{-}3} = 1$ kT units at room temperature.

To this end, we note that the critical values for phase separation in a body-centered cubic ($\kappa = 8$) and a square ($\kappa = 4$) lattices are $\varepsilon_{\kappa=8}^{\text{crit}} = 0.31$ and $\varepsilon_{\kappa=4}^{\text{crit}} = 0.88$.[33] Thus, in our model simulations on the square lattice, we set $\varepsilon_{1\text{-}2} = 0.77$, $\varepsilon_{2\text{-}3} = 0$, and $\varepsilon_{1\text{-}3} = 2.8$ for the system water(1)/NMP(2)/Nomex(3).

Having determined the values of the thermodynamic interaction parameters ε, we turn to an estimation of the kinetic parameters $\tau_{i,j}$, see eq. (1). It is well accepted, from experiments on membrane formation,[34–36] that a polymer in solution does not consist of individual molecules but, rather, of macromolecular aggregates 20 nm in diameter. That aggregation is believed to be caused both by the high polymer concentrations and by the weak solvent power typically used in most coagulation processes. Thus, in our model of elementary particle exchanges on a lattice, we set the unit lattice length $\delta x = 20$ nm. Since the mutual diffusion coefficient of liquids is of the order of 10^{-5}cm^2/s, use of eq. (2) leads to $\tau_{1,2} = 4\ 10^{-7}$ s. The zero-concentration diffusion coefficient of most polymers in good solvents lies in the range 10^{-7}–10^{-6} cm^2/s.[37] Taking $D^{\infty} = 10^{-6.5}$cm^2/s leads to $\tau_{1,3} = \tau_{2,3} = 1.3\ 10^{-5}$ s. Although the polymer concentration varies during the coagulation process, we shall, in our simulations, assume a constancy of the two time constants $\tau_{1,3}$ and $\tau_{2,3}$. That assumption is motivated by the fact that, in the strongly interacting systems under study, the rates of particle exchanges are mainly controlled

by the large changes in the Botzmann factors of the local interaction energies [see eq. (1)].

RESULTS AND DISCUSSION

Having determined all the model parameters, we now turn to a systematic study of the various factors controlling the polymer structure during coagulation.

Skin and Finger Formation

Figure 4 shows the calculated solution/coagulant interface for a 20% solution of Nomex® in NMP after precipitation in water for a time t = 0.02 s. Only the polymer particles have been represented. The figure clearly reveals that the water diffuses inside the polymer solution through a series of finger-like structures. These structures have a strikingly similar shape and originate through regularly spaced pores in a thin skin, in perfect agreement with experimental observation.[10,28] Since our unit lattice spacing is of the order of 20 nm, the skin thickness is estimated to be in the range 0.2–0.3 μm which again conforms with experimental values.[38,39] The

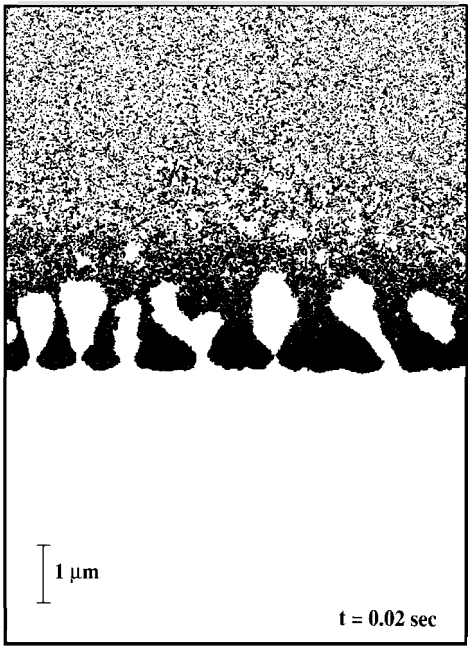

Figure 4. Calculated coagulant/polymer interface for a 20% solution of Nomex® in NMP precipitated in water at t = 0.02 s. The figure is for a square lattice (κ = 4) of 450 × 600 sites; only polymer particles (symbol ●) have been represented. The figure is for $\varepsilon_{1\text{-}2}$ = 0.77, $\varepsilon_{2\text{-}3}$ = 0 and $\varepsilon_{1\text{-}3}$ = 2.8.

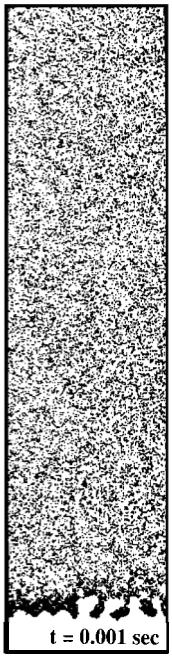

Figure 5. Same as Fig. 4 but, at t = 0.001 s. The figure is for a lattice of 150 × 600 sites.

figure also clearly illustrates the important shrinkage of the polymer film. This is easily visualized by the ca. 5 μm displacement between the actual height of the polymer/coagulant interface and its initial position at the bottom of the figure.

Inspection of our model results leads to the following insight into the origin of the skin/finger formation. Upon immersion of the polymer solution in the coagulation bath, the fast solvent-coagulant exchange across the interface combined with the large repulsive forces between Nomex® and water particles ($\varepsilon_{1\text{-}3}$ = 2.8 kT) cause an immediate precipitation of the polymer at the interface. That process is too fast for any segregation of the polymer into polymer-rich and polymer poor domains and a thin skin starts to form. Since the polymer concentration is low, that early skin is not homogeneous (see Fig. 5), and defects quickly develop along its contour well before the skin has reached its full thickness. Some of these defects form the initiation pores for fingers which then quickly grow inside the polymer solution as it is faster for a solvent particle to exit through a pore than through a defect-free skin. In support of our proposed mechanism for finger formation, we note that fingers are never observed when a skin is absent or, when the polymer volume fraction is too high (i.e., when skin defects are less probable). As the fingers become larger, their number decreases through one of three possible mechanisms: (1)

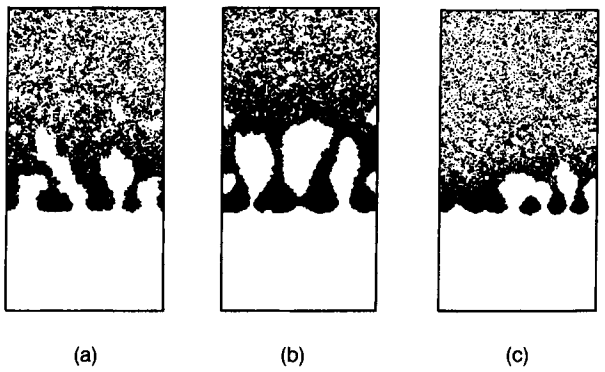

Figure 6. Three possible mechanisms for the decrease in the number of fingers as they grow larger: (A) screening of small fingers by larger ones preventing further growth; (B) closing of the skin pore feeding a finger; (C) lateral merging of neighboring fingers.

screening of small fingers by larger ones preventing further growth (Fig. 6a); (2) closing of the skin pore feeding a finger (Fig. 6b); (3) lateral merging of neighboring fingers. We note that process (3) may be responsible for the experimental observation of multiple pores feeding large fingers.[10] Finger growth eventually stops when the layer of precipitated polymer behind the growing finger tip becomes too dense to be easily broken into. As a last remark, it should be noted that the coagulated finger structures of Figure 4 bear a close resemblance to the viscous fingering instabilities obtained when a fluid of lower viscosity is injected into a more viscous one.[40]

Figure 7 shows concentration profiles at time t = 0.02 sec. for the skin/finger structures of Figure 4. The x-axis represents the distance from the polymer/coagulant interface. As we move from the coagulant/polymer interface toward the uncoagulated polymer solution, the following observations can be made. The skin is typically characterized by a very high polymer concentration, particularly toward its interface with the coagulant. There is, however, almost no solvent present in that layer. As the finger section is entered, the solvent concentration starts to increase. The latter indicates the presence, between fingers, of regions of uncoagulated polymer solution which have been bypassed by the fast-growing fingers. Those regions coagulate more slowly and, hence, eventually lead to sponge-like structures (see later). Note the high polymer concentration ahead of the fingers which keep growing until that fluid polymer layer can no longer be easily moved.[10] Inspection of Figure 7 also shows that the penetration front of coagulant basically coincides with that of the fingers, except for the presence of a few isolated pockets of precipitant deeper inside the polymer solution.

The time dependence of the depth of penetration of the fingers is described in Figure 8. The figure clearly shows that, when distances are squared, the dependence is linear at all times, as observed experimentally.[10,28] Our results therefore indicate that the diffusion of coagulant inside the Nomex® dope almost instantaneously reaches a steady-state re-

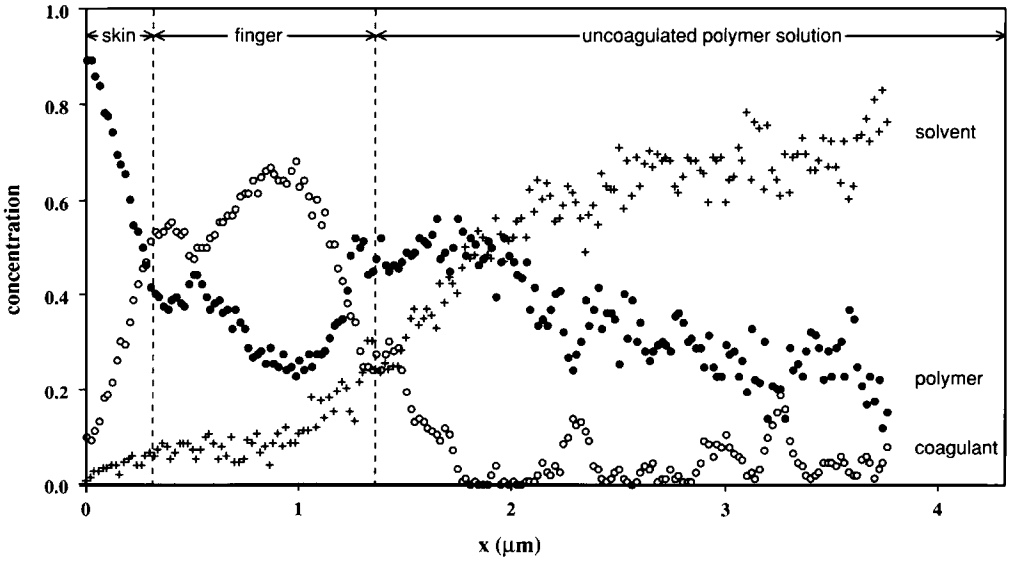

Figure 7. Concentration profiles for a 20% solution of Nomex® in NMP coagulated in water at t = 0.02 s. Calculated data for Nomex®, NMP, and water are denoted by symbols ●, +, and ○, respectively.

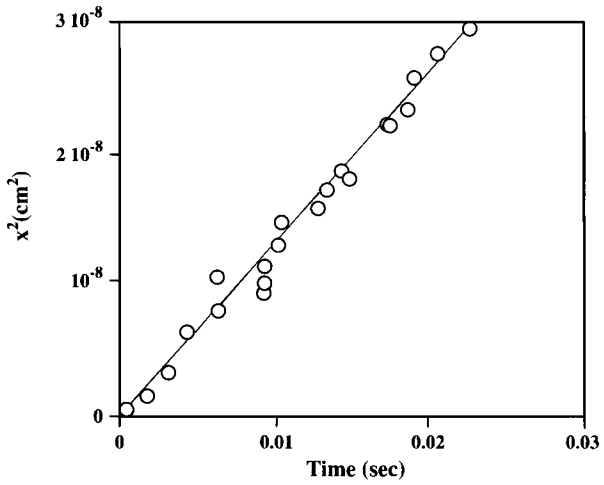

Figure 8. Time dependence of the penetration depth (squared) of the fingers for a 20% solution of Nomex® in NMP coagulated in water (see Fig. 4).

gime. From the figure, we estimate the average diffusion coefficient for the growth of fingers to be around 1.3 10^{-6} cm^2/s. That value is in excellent agreement with the ca. 1.6 10^{-6} cm^2/s estimate that can be extracted from the photomicrographs obtained by Strathmann (Fig. 7 of ref. 28). As will be seen later, these diffusion coefficient values are rather high and they are typical of all finger-like polymer structures.

Effect of the Solvent/Coagulant Miscibility

The miscibility of the solvent and coagulant is, in our model, controlled by the interaction energy parameter $\varepsilon_{1\text{-}2}$. Figure 9a–d show a series of polymer structures obtained at increasing values of $\varepsilon_{1\text{-}2}$. All the figures are for approximately the same time t = 0.02–0.03 s. In the absence of any heat of mixing of the solvent with the coagulant ($\varepsilon_{1\text{-}2}$ = 0, Fig. 9a), the polymer is seen to coagulate into large agglomerates of ca. 0.3 μm in diameter (dustlike structure). Although the agreement may be fortuitious, it is interesting to note that the latter value is close to our estimation of the skin thickness (Fig. 4) and also to the diameter of the secondary particles observed during coagulation of cellulose-acetate membranes.[35] As the miscibility of solvent and coagulant decreases ($\varepsilon_{1\text{-}2}$ = 0.5 and $\varepsilon_{1\text{-}2}$ = 0.77, Figs. 9b and 9c), we observe the development of finger-like structures which also become more regular as $\varepsilon_{1\text{-}2}$ increases. Finally, for very immiscible solvent and coagulant ($\varepsilon_{1\text{-}2}$ = 1.5, Fig. 9d), a very dense polymer structure is obtained in which the coagulant starts forming spherical pores (sponge-like structure) behind the skin. It is interesting to note that the sequence of morphologies obtained in Figure 9 through a decrease in solvent/coagulant miscibility is also very similar to that obtained experimentally[10] through an increase in the initial polymer concentration. This is easily understandable since a decrease in solvent/coagulant miscibility effectively makes solvent and polymer particles more alike as far as the coagulant is concerned.

As has been widely anticipated in the literature, the transition from sponge to finger to dust-like structures is also accompanied by a dramatic increase of the rate of coagulation. This is clearly exemplified by the results of Figure 10 which show the

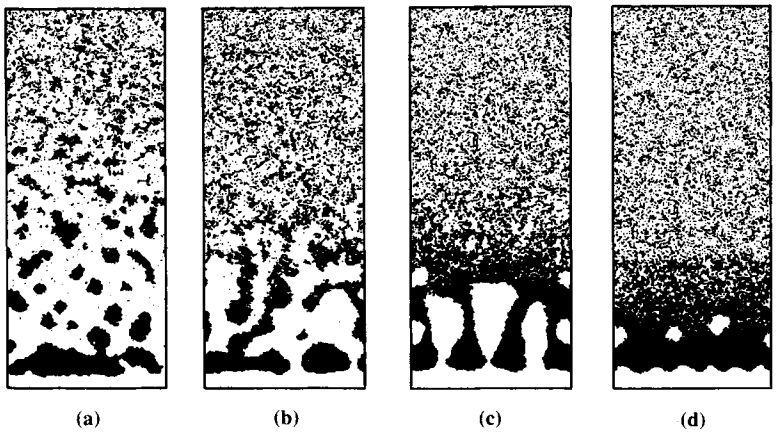

Figure 9. Effect of the solvent/coagulant miscibility on polymer structure. (a): $\varepsilon_{1\text{-}2}$ = 0; (b): $\varepsilon_{1\text{-}2}$ = 0.5; (c): $\varepsilon_{1\text{-}2}$ = 0.77; and (d): $\varepsilon_{1\text{-}2}$ = 1.5. The structures are for a coagulation time t = 0.02 s, except (d) which is for t = 0.03 s. All the other parameters are the same as in Fig. 4. The extent of shrinking of the polymer/coagulant interfaces with respect to their initial positions has not been represented.

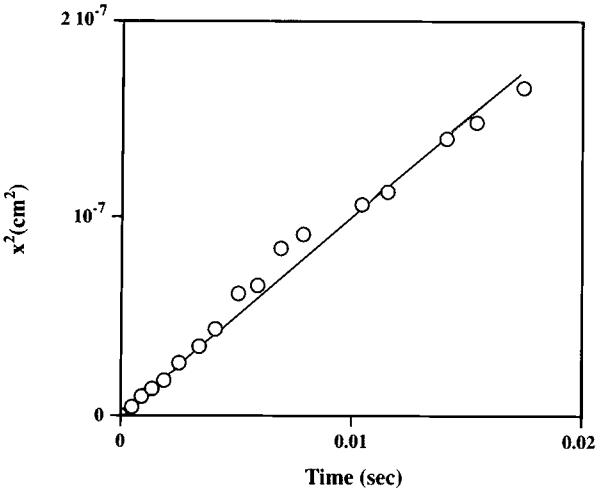

Figure 10. Time dependence of the penetration depth (squared) of the coagulation front for the system studied in Fig. 9a.

time dependence of the penetration depth (squared) of the coagulation front for the dust-like structure studied in Figure 9a. Again the dependence is clearly linear at all times and a diffusion coefficient of ca. 10^{-5} cm^2/s is easily obtained. Comparing with the results of Figure 8, that value is an order of magnitude higher than the diffusion coefficient for the finger-like structure of Figure 9c. Further investigation also reveals a two orders of magnitude difference with the sponge-like structure of Figure 9d, for which a diffusion coefficient of ca. 2 10^{-7} cm^2/s is found.

Effect of the Coagulant Strength

We now turn to study the effect of coagulant strength through varying the interaction energy $\varepsilon_{1\text{-}3}$ between coagulant and polymer. The results are presented in Figure 11a–d for a coagulation time t = 0.03 s. When the coagulant is weak ($\varepsilon_{1\text{-}3}$ = 1, Fig. 11a), a partial dissolution of the polymer into the coagulating bath is observed with no skin formation at the coagulant/polymer interface. That morphology is further studied in Figure 12 which clearly reveals a rather diffuse coagulant/polymer interface with no evidence for a polymer skin. Figure 12 also shows that the concentration of coagulant within the polymer solution is rather uniform (compare with Fig. 7). At t = 0.03 s, that concentration is, however, still too low to cause any precipitation of the polymer. For the present case with $\varepsilon_{1\text{-}3}$ = 1, precipitation is expected to occur at coagulant concentrations above 46%. Thus, polymer coagulation in Figure 11a should be an extremely slow process controlled entirely by particle nucleation and growth and leading eventually to a uniform sponge-like structure with no skin.

As the coagulant power is slightly increased ($\varepsilon_{1\text{-}3}$ = 1.5, Fig. 11b), the coagulation rate improves and some polymer precipitation is now observed at t = 0.03 s. The figure shows the formation of a very thin skin below which a sponge-like polymer structure starts to develop. Even though the penetration depth of the coagulation front is rather small, a crude analysis of the results of Figure 11b leads to a diffusion coefficient of ca. 2. 10^{-7} cm^2/s, a value almost

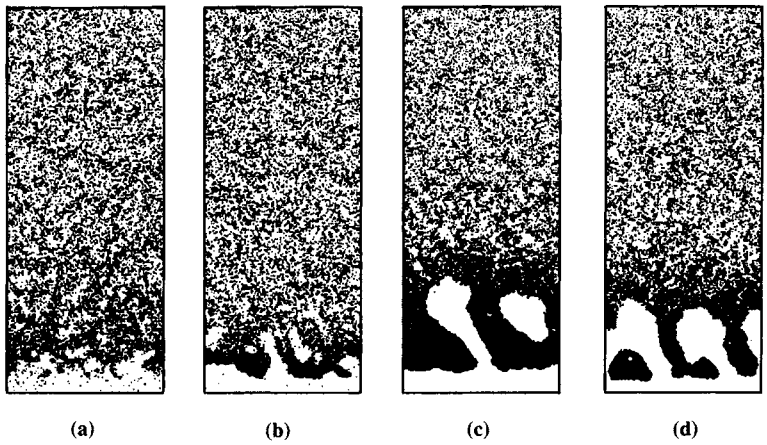

Figure 11. Effect of the coagulant strength on polymer structure. (a): $\varepsilon_{1\text{-}3}$ = 1; (b): $\varepsilon_{1\text{-}3}$ = 1.5; (c): $\varepsilon_{1\text{-}3}$ = 4; and (d): $\varepsilon_{1\text{-}3}$ = 6. The structures are for a coagulation time t = 0.03 s. All the other parameters are the same as in Fig. 4. The extent of shrinking of the polymer/coagulant interfaces with respect to their initial positions has not been represented.

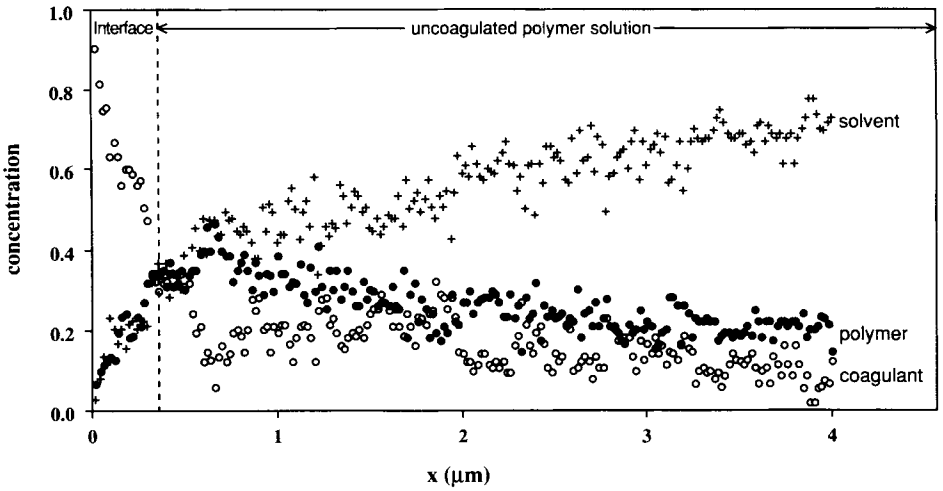

Figure 12. Concentration profiles for the polymer structure depicted in Fig. 11a. Calculated data for the polymer, solvent, and coagulant are denoted by symbols ●, +, and ○, respectively.

two orders of magnitude lower than that calculated for Figure 9a. These results, again, stress the importance of the coagulation rate in controlling the final polymer structure.

For very strong coagulants ($\varepsilon_{1\text{-}3} = 4$ and $\varepsilon_{1\text{-}3} = 6$, Fig. 11c–d), the coagulation rate increases and, as expected, a transition to a finger-like structure is observed. We note, however, that we have been unable through further increases in $\varepsilon_{1\text{-}3}$ to observe a second transition to a dust-like structure (Fig. 9a). The latter, therefore, seems to be typical of systems in which the coagulant and the solvent have a low heat of mixing.

CONCLUSIONS

We have presented a computer model for the study of the development of structure during coagulation of a polymer dope. In our approach, the coagulation process is simulated on a lattice whose sites represent either a coagulant, a solvent or a polymer particle. Diffusion is described through a Monte Carlo process of particle exchanges on nearest neighbor lattice sites, the probability for a single event being weighted by the Boltzmann exponent of the change in local energy. These energy changes are themselves obtained from a set of pair interaction parameters that are easily extracted from binary mixture data.

Our model has allowed, for the first time, to describe the coagulation process beyond the initial quench state and to reproduce the wide variety of different polymer structures that can be obtained, ranging from dust- to finger- to sponge-like morphologies. We have shown that those morphologies are fully controlled by the coagulation rate which varies by almost two orders of magnitude between dust- and sponge-like structures. The coagulation rates were themselves found to be very sensitive to variations in the coagulant power and in the coagulant/solvent miscibility.

Admittedly, our results are for short coagulation times ($t < 0.03$ s) which has allowed the study of structures no larger than a few microns in depth. In that respect, it is worth noting that the structures presented in Figures 6 and 9 already take several weeks CPU time each on a 25 MHz processor of a 280 SGI server. Since the depth of the coagulation front increases linearly with the square-root of time (see Figs. 8 and 10), the CPU time required for much larger structures becomes prohibitively too large. It could be argued that, being for small coagulation times $t < 0.03$ s, the results of the present paper are not representative of the fully coagulated structures that sometimes require up to a few minutes to obtain. In support of our results, it is worth noting that actual photomicrographs[10] of coagulation patterns obtained at different times, ranging from a few seconds to several minutes, do not reveal any evidence for a change in polymer structure with time (see also Figs. 4 and 5 in that connection). In addition, our results of Figures 8 and 10 clearly indicate that the diffusion coefficient of the coagulation front remains fairly constant with time. Since the value of

that coefficient fully dictates the structure of the coagulated polymer, a change in morphology at later times remains improbable and the gross morphology of the final polymer structure should be adequately described by our model results.

REFERENCES AND NOTES

1. W. E. Dorogy and A. K. St. Clair, *J. Appl. Polym. Sci.*, **43,** 501 (1991).
2. G. C. Gross, DuPont Progress Report, HT 68-7 (1968).
3. J. E. Van Trump, DuPont Progress Report, PR 90-24 (1990); PR 92-11 (1992).
4. R. E. Kesting, *Synthetic Polymeric Membranes,* J. Wiley & Sons, N.Y., 2nd Ed. (1985).
5. R. Matz, *Desalination,* **10,** 1 (1972).
6. M. Frommer and R. Messalem, *Ind. Eng. Chem., Prod. Res. Dev.*, **12**(4), 328 (1973).
7. L. E. Scriven and C. U. Sternling, *Nature,* **187,** 186 (1960).
8. R. J. Ray, W. B. Krantz, and R. L. Sani, *J. Membr. Sci.*, **23,** 155 (1985).
9. P. Neogi, *AIChE J.*, **29,** 402 (1983).
10. H. Strahmann, K. Kock, P. Amar, and R. W. Baker, *Desalination,* **16,** 179 (1975).
11. J. E. Anderson and R. Ullman, *J. Appl. Phys.*, **44,** 4303 (1973).
12. C. Cohen, G. B. Tanny, and S. Prager, *J. Polym. Sci.: Polym. Phys. Ed.*, **17,** 477 (1979).
13. J. G. Wijmans, F. W. Altena, and C. A. Smolders, *J. Polym. Sci.: Polym. Phys. Ed.*, **22,** 519 (1984).
14. A. J. McHugh and L. Yilmaz, *J. Polym. Sci.: Polym. Phys. Ed.*, **23,** 1271 (1985).
15. A. J. Reuvens, F. W. Altena, and C. A. Smolders, *J. Polym. Sci.: Polym. Phys. Ed.*, **24,** 793 (1986).
16. A. J. Reuvens, J. W. A. van den Berg, and C. A. Smolders, *J. Membr. Sci.*, **34,** 45 (1987).
17. A. J. Reuvens and C. A. Smolders, *J. Membr. Sci.*, **34,** 67 (1987).
18. L. Yilmaz and A. J. McHugh, *J. Membr. Sci.*, **28,** 287 (1986).
19. A. J. McHugh and L. Yilmaz, *J. Membr. Sci.*, **43,** 319 (1989).
20. C. S. Tsay and A. J. McHugh, *J. Polym. Sci.: Polym. Phys. Ed.*, **28,** 1327 (1990).
21. T. L. Hill and O. Kedem, *J. Theor. Biol.*, **10,** 399 (1966).
22. R. Gordon, *J. Chem. Phys.*, **49,** 570 (1968).
23. Z. Alexandrowicz and Y. Termonia, *Molec. Phys.*, **38,** 47 (1979).
24. Y. Termonia, *Molec. Phys.*, **38,** 65 (1979).
25. Y. Termonia and Z. Alexandrowicz, *Molec. Phys.*, **39,** 725 (1980).
26. Y. Termonia, *Phys. Rev. Letters,* **72,** 3678 (1994).
27. M. A. Frommer and D. Lancet, in *Reverse Osmosis Membrane Research,* H. K. Lonsdale and H. E. Podall, eds., Plenum Press, New York, 1972, p. 85.
28. H. Strathmann, in *Materials Science of Synthetic Membranes,* ACS Symposium Series, 269, 165 (1985).
29. Y. Termonia, P. Meakin, and P. Smith, *Macromolecules,* **18,** 2246 (1985).
30. P. Meakin, *Phys. Rev. Lett.*, **51,** 1119 (1983).
31. Y. Termonia, unpublished results.
32. The error involved in fitting the theoretical spinodal curve to the experimental binodal line is not expected to be of importance since, in those highly immiscible systems, binodal and spinodal curves are close to each other.
33. C. Domb, *Adv. Phys.*, **9,** 149 (1960).
34. R. E. Kesting, *J. Appl. Polym. Sci.* **41,** 2739 (1990).
35. K. Kamide and S. Manabe, in *Materials Science of Synthetic Membranes,* ACS Symposium Series, 269, 197 (1985).
36. M. Panar, H. H. Hoehn, and R. R. Hebert, *Macromolecules,* **6,** 777 (1973).
37. Polymer Handbook, J. Brandrup and E. H. Immergut, eds., 2nd Ed., John Wiley & Sons, New York, 1975.
38. R. L. Riley, J. O. Gardner, and U. Merten, *Desalination,* **1,** 30 (1966).
39. H. K. Lonsdale, U. Merten, and R. L. Riley, *J. Appl. Polym. Sci.*, **9,** 1341 (1965).
40. J. Nittmann, G. Daccord, and H. E. Stanley, *Nature* **314,** 141 (1985); D. Bensimon, L. P. Kadanoff, S. Liang, B. I. Shraiman, and C. Tang, *Rev. Mod. Phys.* **58,** 977 (1986); E. Ben-Jacob and P. Garik, *Nature* **343,** 523 (1990); K. R. Bhaskar, P. Garik, B. S. Turner, J. D. Bradley, R. Bansil, H. E. Stanley, and J. T. LaMont, *Nature,* **360,** 458 (1992).

Received May 11, 1994
Revised July 19, 1994
Accepted August 10, 1994